Journal of Sustainability Science and Management
Volume 19 Number 12, December 2024: 58-73
eISSN: 2672-7226

JOULE HEATING, THERMAL RADIATION, AND SLIP EFFECTS ON MAGNETOHYDRODYNAMIC FLOW AND HEAT TRANSFER OVER AN EXPONENTIALLY STRETCHING/SHRINKING SHEET IN FERROFLUIDS

NORSHAFIRA RAMLI[1]*, AHMAD SYAKIR MOHD SHAFRI[2] AND NUR SYAZANA ROSLY[3]

[1]School of Mathematical Sciences, Universiti Sains Malaysia, 11800 Gelugor, Penang, Malaysia. [2]Department of Mathematics, Faculty of Science, Universiti Teknologi Malaysia, 81310 Skudai, Johor Bahru, Johor, Malaysia. [3]Centre of Foundation Studies, Universiti Teknologi MARA, Selangor Branch, Dengkil Campus, 43800 Dengkil, Selangor, Malaysia.

**Corresponding author: norshafiraramli@usm.my*
http://doi.org/10.46754/jssm.2024.12.004
Received: 6 August 2023 *Accepted: 8 June 2024* *Published: 15 December 2024*

Abstract: This research was carried out to study the constant bi-dimensional (2D) MHD flow and thermal energy exchange of ferrofluids with respect to an exponentially stretched or shrunk sheet, as well as the influences of slip, thermal radiation, and Joule heating. Before numerical analysis using the shooting technique, the translation of the governing (or principal) partial equations to the group of non-linear ordinary differential equations using a similarity transformation was performed. By using graphs and tables, the significances of several relevant parameters (i.e., radiation, magnetic, mass transmission, slip, and stretching or shrinking variables with the Eckert number) on Nusselt number, temperature profile, and velocity, as well as the common coefficient of skin friction were examined. Non-unique or dual solutions were encountered in the value range of practised parameters for stretching and shrinking. The results proved that the increment of the magnetic, radiation, mass transfer (suction), slip parameters, and Eckert number will accelerate the heat transfer rate.

Keywords: Joule heating, thermal radiation, exponentially stretching/shrinking, magnetohydrodynamic, ferrofluid.

Introduction

Convectional heat transfer fluids with poor thermal conductivity such as ethylene glycol, oil, and water may substantially impair the capability of abundant engineering equipment such as boilers, steam generators, and electrical appliances. In order to get around this problem, numerous attempts have been made to replace the liquids used for heat transfer with those with a more sophisticated heat conduction. Ferrofluids are an ideal innovative technique to boost the conductivities of the fluids' thermal properties. Ferrofluids comprise single-domain particles of ferromagnetic suspended in a non-magnetic transporting fluid. To maintain a sustainable interruption condition, the particles, typically 10 nm or smaller in diameter are covered in layers of absorbed surfactant. Examples of ferrofluids include magnetite (Fe_3O_4), hematite (Fe_2O_4), cobalt ferrite ($CoFe_2O_4$), and manganese-zinc ferrite (Mn - $ZnFe_2O_4$), which are ion-based ferroparticles. This particular type of ferrofluid has numerous potential applications in the fields of biomedicine, energy conversion systems, radioactive chemicals, and water purification along with mechanoelectrical applications such as semiconductors, drug delivery, and Magnetic Resonance Imaging (MRI) (Blaney, 2007; Sharifi *et al.*, 2012). In the 1960s, National Aeronautics and Space Administration (NASA) invented ferrofluids for space applications (Stephen, 1965). The synthesis and applications of ferrofluids were the subject of former investigations by Rosensweig (1985) and Raj and Moskowitz (1990).

Ferrofluids offer a huge potential for heat transfer applications due to their properties, their strength of magnetic field and the alterability of their temperature distribution. Lajvardi *et al.* (2010) conducted an experimental evaluation of the heat transmission of Fe_3O_4 in a heated copper tube. Accredited to the thermo-physical

properties of ferrofluid such as its excellent heat conductivity, beneath a magnetic field, the heat transfer coefficient has been significantly improved. Alsaady *et al.* (2015) highlighted how the external magnetic field influenced the thermophysical properties of ferrofluid and its relative augmentation in thermomagnetic convention. They found that applying an external magnetic field can improve forced convective heat transfer as opposed to not having a magnetic field only under specific boundary conditions.

Fadaei *et al.* (2017) examined how the magnetic field affected the improvement of heat transfer in Fe_3O_4 ferrofluids. They found that the fluid mixing may be enhanced by applying a magnetic field, raising the Nusselt number value along the pipe's length. Additionally, Ramli *et al.* (2017), Gui *et al.* (2018), Khosravi *et al.* (2019), Asadi *et al.* (2019), Ramli and Ahmad (2021), Olayemi *et al.* (2022), Cao *et al.* (2023), and Farooq *et al.* (2023) did a few studies on improving heat transfer with ferrofluids in the manifestation of exterior magnetic field. Ferrofluids are also essential for absorbing electromagnetic fields to improve heat transmission.

Researchers are interested in studying boundary layer flow and heat transmission in overstretched or shrunk layers. This is due to its enormous significance in a variety of engineering and industrial processes such as the extraction of rubber sheet and polymer, the tinning and annealing of copper wires, the production of glass fibre, the growth of crystals, continuous filament pulling through idle fluid, and hot rolling (Aly & Ebaid, 2013; Reddy, 2014; Abbas *et al.*, 2016). Jusoh *et al.* (2018) investigated the effects of exponentially stretching or shrinking sheets on the 3D rotational flow of ferrofluids and heat transfer. A drag force was produced on the surface of the shrinking sheet, directly proportional to the increment of the rotational parameter. In their investigation of the heat transfer and magnetohydrodynamic flow of ferrofluids across a sheet that is exponentially stretching or shrinking, Rasli and Ramli (2021) emphasised that the addition of ferroparticles significantly increases the fluids' thermal conductivity and rate of heat transmission. The implementation of MHD and a heat source or sink for the stagnation point region was carried out by Anuar *et al.* (2021) using a hybrid ferrofluid over an exponentially stretching or shrinking surface. They concluded that heat absorption is most likely to occur on the sheet in the case of a stronger heat source. By taking into account the effect of velocity slip, this was later expanded by Zainodin *et al.* (2022) for the mixed convection in hybrid ferrofluid. Stronger heat sinks and stretching parameters produce better heat transfer results, whereas heat sources and shrinking parameters produce the opposite results. Skin friction and fluid flow are affected by the presence of velocity slip.

The process of producing heat on a conductor using an electric current is known as Joule heating. Electric heaters, resistance ovens, and iron-cooked meals are merely a few examples of the instruments and industries that utilise joule heating. Sajid *et al.* (2016) investigated the magnetohydrodynamic and Joule heating impacts of the flow of Fe_3O_4 ferrofluid in a semi-porous curved channel. The temperature distribution was shown to have increased in response to an increase in Eckert number.

Furthermore, Kumar *et al.* (2021) reported on the heat transfer of current-transporting microwire in ferrofluid and the influence of the axisymmetric magnetic field's potential. The effects of frictional heating and Joule's dissipation concerning non-Newtonian ferrofluid flow across a bidirectionally extended convective surface were also studied by Reddy *et al.* (2018). The peristaltic motion of ferrofluids in a plumb conduit under conditions of fluid friction and Joule heating was investigated by Abrar *et al.* (2019) using an entropy formation analysis. They discovered that raising the Joule heating parameter may cause an increase in fluid temperature. Several scholars have conducted additional research on the Joule heating effect in ferrofluid using other parameters, including Kumar *et al.* (2017), Abdel-Wahed (2017), and Mittal *et al.* (2019).

The effect of heat radiation on the exchange of heat in ferrofluids has become crucial due to their versatility for high-temperature processes and space technology. Chamkha *et al.* (2003) examined how thermal radiation with a heat source or sink impacted MHD over an un-isothermic wedge. The wedge's surface is believed to be porous, which will enable potential injection or suction of the wall. The thermal radiation parameter was inversely proportional to the local Nusselt number. The function of heat radiation in the presence of Lorentz forces by considering the changing ferrofluid viscosity has been proved by the study made by Sheikholeslami and Shehzad (2017). They came up with the answer by taking into thought the Fe_3O_4 ferroparticles that were present in the aqueous fluid. The findings showed that the radiation variables were directly proportional to the interior wall temperature.

Rashad (2017) studied the effect of thermal radiation on the MHD slip flow of a ferrofluid over an un-isothermic wedge. The findings demonstrated that the skin friction coefficient exhibits a non-conflicting pattern for all examined values of the heat radiation parameter. Jamaludin *et al.* (2020) investigated the Fe_3O_4-water ferrofluid diversified convective flow towards a non-stationary surface under the influence of heat radiation and MHD. It was discovered that thermal radiation and the degree of heat transfer were inversely related. Siddiqui *et al.* (2023) observed the effects of thermal radiation and heat reaction on MHD convective flow in the ferrofluid concentrated "*I-shaped*" cavity. A large number of researchers have also reviewed different geometries related to ferrofluid, including Jue (2006), Raju *et al.* (2015), Raju and Sandeep (2016), Mustafa *et al.* (2016), Babu *et al.* (2016), Ramli and Ahmad (2019), Khashi'ie *et al.* (2022), Wan Rosli *et al.* (2023), and Gerdroodbary *et al.* (2023).

Several researchers have been keen on heat transfer and magnetohydrodynamic flow. However, their concerns were not mainly confined to ferrofluids. Motivated by the studies from Rasli and Ramli (2021) and Khashi'ie *et al.* (2022), this current study is to provide a thorough analysis of the effects of thermal radiation, slip, and Joule heating on heat transfer and magnetohydrodynamic flow over an exponentially stretching or shrinking sheet in ferrofluids. We believe that as this work has not been investigated before, the facts ought to be mentioned. Additionally, the issue formulation in the current study was done using the shooting method in the Maple software. As with the exponentially stretching or shrinking sheet, the approach above has established multiple successful solutions. The investigation outcomes for particular situations are compared to those reported in the literature to confirm the accuracy of the numerical answers.

Basic Equations

Consider a continuous, two-dimensional, laminar, incompressible flow of magnetohydrodynamic (MHD) and heat transfer of ferrofluids over an exponentially stretched or shrunk sheet while taking slip, Joule heating, and thermal radiation into account. Figure 1 shows a schematic illustration of flow geometry.

Water-based ferrofluids made of cobalt ferrite ($CoFe_2O_4$), magnetite (Fe_3O_4), and manganese-zinc ferrite (Mn - $ZnFe_2O_4$) were the fluids under investigation. The stretching or shrinking surface's velocity distribution is supposed to be $U_w(x) = ae^{x/L}$, where x is the coordinate measured along the surface, L is the sheet's length, and a is a constant, where $a > 0$ for a stretching sheet and $a < 0$ for a shrinking sheet. Additionally, it is assumed that the continuous mass flux velocity is v_0, where $v_0 < 0$ for mass suction and $v_0 > 0$ for mass fluid injection.

The following equations provide the governing equations for the ferrofluid, where the order of magnitude analysis was used and the premises above were taken into account (Shah *et al.*, 2016; Yashkun *et al.*, 2020; Rasli & Ramli, 2021):

$$\frac{\partial u}{\partial x} + \frac{\partial v}{\partial y} = 0, \quad (1)$$

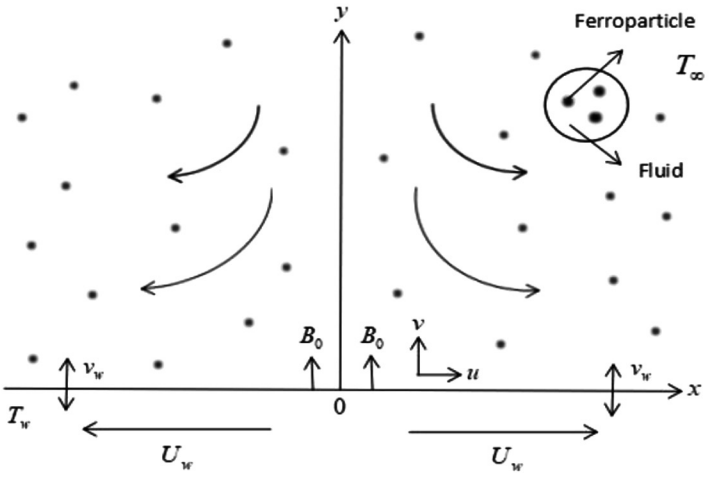

(a) Stretching sheet

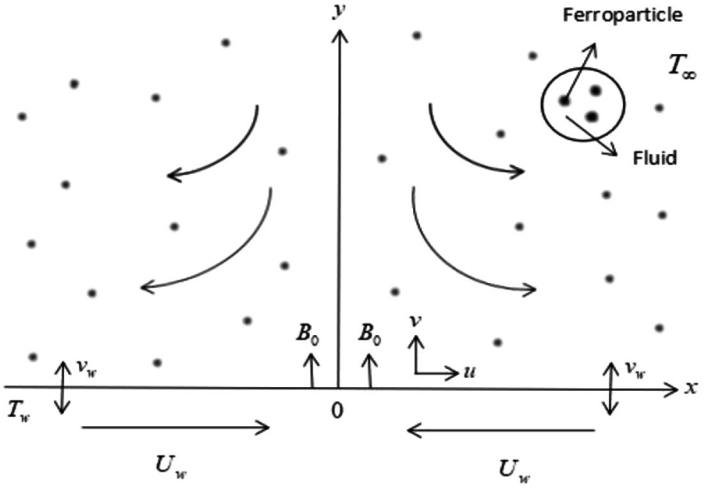

(b) Shrinking sheet

Figure 1: A schematic representation of flow geometry

$$u\frac{\partial u}{\partial x}+v\frac{\partial u}{\partial y}=\frac{\mu_{ff}}{\rho_{ff}}\frac{\partial^2 u}{\partial y^2}-\frac{\sigma_{ff}B^2}{\rho_{ff}}u, \tag{2}$$

$$u\frac{\partial T}{\partial x}+v\frac{\partial T}{\partial y}=\frac{k_{ff}}{\left(\rho C_p\right)_{ff}}\frac{\partial^2 T}{\partial y^2}-\frac{1}{\left(\rho C_p\right)_{ff}}\frac{\partial q_R}{\partial y}+\frac{\sigma_{ff}B^2}{\left(\rho C_p\right)_{ff}}u^2, \tag{3}$$

Liable to be subjected via the boundary conditions:

$$u=\lambda\, U_w(x)+N\frac{\partial u}{\partial y},\quad v=v_w,\quad T=T_w=T_\infty+T_0e^{x/2L}\quad \text{at}\quad y=0,$$
$$u\to 0,\quad T\to T_\infty\quad \text{as}\quad y\to\infty. \tag{4}$$

where u and v represent the components of velocity through the x- and y- axes, respectively, σ_{ff} is an electrical conductivity of ferrofluid, B is the sum of the magnetic field, T is the surface layer temperature, q_R is the radiative heat flux, U_w is the stretching or shrinking velocity, $N = N_1 e^{-x/2L}$ is the slip factor with N_1 is the initial value of slip factor, v_w is the variable wall mass transfer velocity, T_w is the variable surface temperature, and T_∞ is the free stream temperature, anticipated to be constant.

Here, μ_{ff} is the dynamic viscosity of the ferrofluid, ρ_{ff} is the density of the ferrofluid, k_{ff} is the thermal conductivity of the ferrofluid, and $(\rho C_p)_{ff}$ is the heat capacity of the ferrofluid, which are defined as follows:

$$\nu_{ff} = \frac{\mu_{ff}}{\rho_{ff}},\ \mu_{ff} = \frac{\mu_f}{(1-\varphi)^{2.5}},\ \alpha_{ff} = \frac{k_{ff}}{(\rho C_p)_{ff}},\ \rho_{ff} = (1-\varphi)\rho_f + \varphi\rho_s,$$
$$(\rho C_p)_{ff} = (1-\varphi)(\rho C_p)_f + \varphi(\rho C_p)_s, \frac{k_{ff}}{k_f} = \frac{(k_s + 2k_f) - 2\varphi(k_f - k_s)}{(k_s + 2k_f) + \varphi(k_f - k_s)}. \quad (5)$$

where μ_f is the viscosity of the fluid, φ is the ferroparticle volume fraction, k_f and k_s accordingly denote the fluid and solid thermal conductivities, besides ρ_f and ρ_s denote their density, respectively. The variable magnetic field $B(x)$ is taken in the form:

$$B(x) = B_0 e^{x/2L}, \quad (6)$$

where, B_0 is a constant magnetic field. Meanwhile, v_w is the variable wall mass transfer velocity and is given by:

$$v_w = v_0 e^{x/2L}. \quad (7)$$

The radiative heat flux is summarised as follows, based on Rosseland's approximation for radiation:

$$q_R = -\frac{4\varepsilon}{3\varrho}\frac{\partial T^4}{\partial y}, \quad (8)$$

where ϱ and ε are expressed as the mean absorption and the Stefan-Boltzmann constant, respectively. In addition, the temperature variations within the flow are expected to allow for a linear expression of the term T^4. As a result, by omitting higher-order terms and expanding T^4 in a Taylor series about T_∞, we obtain:

$$T^4 \approx 4{T_\infty}^3 - 3{T_\infty}^4. \quad (9)$$

Using Equations (8) and (9), Equation (3) reduces to:

$$u\frac{\partial T}{\partial x} + v\frac{\partial T}{\partial y} = \left(\alpha_{ff} + \frac{1}{(\rho C_p)_{ff}}\frac{16\varepsilon {T_\infty}^3}{3\varrho}\right)\frac{\partial^2 T}{\partial y^2} + \frac{\sigma_{ff}B^2}{(\rho C_p)_{ff}}u^2, \quad (10)$$

where $\alpha_{ff} = k_{ff}/(\rho C_p)_{ff}$ stands for the thermal diffusivity. Consequently, we embrace $R = 4\varepsilon T_\infty / k_{ff}\varrho$ indicates a radiation parameter, Equation (10) becomes:

$$u\frac{\partial T}{\partial x} + v\frac{\partial T}{\partial y} = \alpha_{ff}\left(1 + \frac{4R}{3}\right)\frac{\partial^2 T}{\partial y^2} - \frac{\sigma_{ff}B^2}{(\rho C_p)_{ff}}u^2, \quad (11)$$

By incorporating the subsequent similarity transformation, the governing Equations (1), (2), and (11) subject to the boundary constraints (4) can be written in a simpler manner:

$$\eta = y\left(\frac{a}{2\nu_f L}\right)^{1/2} e^{x/2L}, \quad \psi = \left(2\nu_f L a\right)^{1/2} f(\eta) e^{x/2L}, \quad \theta(\eta) = \frac{T - T_\infty}{T_w - T_\infty}, \tag{12}$$

where η denotes the similarity variable, ν_f denotes the kinematic viscosity of the base fluid, ψ stands for the stream function defined as $u = \partial\psi/\partial y$, and $v = \partial\psi/\partial y$. Thus, we have:

$$u = a e^{x/L} f'(\eta), \quad v = -\sqrt{\frac{\nu_f a}{2L}}\, e^{x/2L}[f(\eta) + \eta f'(\eta)]. \tag{13}$$

Equations (2) and (11) simplify to the following nonlinear ordinary differential equations when the similarity variables (12) are employed:

$$\frac{1}{(1-\varphi)^{2.5}\left(1-\varphi+\varphi\rho_s/\rho_f\right)} f''' + f f'' - 2(f')^2 - \frac{\sigma_{ff}/\sigma_f}{1-\varphi+\varphi\rho_s/\rho_f} M f' = 0, \tag{14}$$

$$\frac{k_{ff}/k_f}{1-\varphi+\varphi\left(\rho C_p\right)_s/\left(\rho C_p\right)_f} \frac{1}{\Pr}\left(1+\frac{4R}{3}\right)\theta'' + f\theta' - f'\theta + \frac{\sigma_{ff}/\sigma_f}{1-\varphi+\varphi\left(\rho C_p\right)_s/\left(\rho C_p\right)_f} M \,\mathrm{Ec}\,(f')^2 = 0, \tag{15}$$

where primes denote differentiation η concerning, $M = 2\sigma_f B_0{}^2 L/\rho_f a$ is the magnetic parameter, $\Pr = (\mu C_p)_f/k_f$ is the Prandtl number, and $\mathrm{Ec} = U_w{}^2/\left[(T_w - T_\infty)(c_p)_f\right]$ is Eckert number. The boundary conditions in Equation (4) reduce to the following form:

$$f(0) = S, \quad f'(0) = \lambda + \gamma f''(0), \quad \theta(0) = 1, \quad f'(\eta) \to 0, \quad \theta(\eta) \to 0 \quad \text{as} \quad \eta \to \infty, \tag{16}$$

in such that $S = -v_0\sqrt{2L/\nu_f a}$ is the wall mass transfer parameter, where $S > 0$ resembles to suction and $S < 0$ resembles to injection. Moreover, the stretching or shrinking parameter is signified as λ with regards to $\lambda > 0$ for a stretching sheet and $\lambda < 0$ for a shrinking sheet, along with $\gamma = N_1\sqrt{a/2\nu_f L}$ denotes the slip parameter.

The skin friction coefficient C_f and the local Nusselt number Nu_x, which are physical quantities of relevance are determined as:

$$C_f = \frac{\tau_w}{\rho_f U_w{}^2}, \quad Nu_x = \frac{L\, q_w}{k_f(T_w - T_\infty)}, \tag{17}$$

where the surface shear stress τ_w and the surface heat flux q_w are given by:

$$\tau_w = \mu_{ff}\left(\frac{\partial u}{\partial y}\right)_{y=0}, \quad q_w = -\left(k_{ff} + \frac{16\varepsilon T_\infty{}^3}{3\varrho}\right)\frac{\partial T}{\partial y}_{y=0}. \tag{18}$$

The similarity variables (12) allow us to derive:

$$(2\mathrm{Re})^{1/2}\, C_f = \frac{1}{(1-\varphi)^{2.5}} f''(0), \tag{19}$$

$$(2/\mathrm{Re})^{1/2}\, Nu_x = -\frac{k_{ff}}{k_f}\left(1+\frac{4R}{3}\right)\theta'(0), \tag{20}$$

where $\mathrm{Re} = (U_w L)/\nu_f$ is the Reynolds number.

Results and Discussion

Using the shooting technique, a numerical analysis of the boundary-constrained nonlinear ordinary differential Equations (14) and (15) has been done. An in-depth discussion will be held regarding the impact of various values of the magnetic parameter M, radiation parameter R, slip parameter γ, Eckert number Ec, mass transfer parameter S, and stretching or shrinking λ sheet parameter on the coefficient skin friction $f''(0)$, local Nusselt number $-\theta'(0)$, in addition to velocity and temperature profiles.

In terms of the Prandtl number, it is set to 6.2. The volume fraction of solid ferroparticles is considered to be in the range of $0 \leq \varphi \leq 0.2$, which $\varphi = 0$ corresponds to pure fluid water. The ferrofluids' thermophysical properties are shown in Table 1 and were derived from Ramli *et al.* (2018) and Ramli and Ahmad (2021). The current findings are compared to those of Waini *et al.* (2020) and Yashkun *et al.* (2020) in Table 2 to assess the feasibility of numerical results. The results show excellent agreement with each other.

The diversities in the skin friction coefficient $f''(0)$, local Nusselt number $-\theta'(0)$ under physical parameters M and S are portrayed in Figures 2 to 5. It is apparent that dual solutions (first and second solutions) subsist for Equations (14) to (16) throughout the interval of $\lambda > \lambda_c$, where λ_c is a critical value of λ. Additionally, no solution has been discovered for $\lambda < \lambda_c$. It is important to note that Yasin *et al.* (2015) and Waini *et al.* (2020) have considered the possibility of dual solutions for the basic ordinary differential equations. The first solution was stable, whereas the latter was not due to the disturbances caused by the moderately negative eigenvalues. Therefore, the second solution was considered of no physical importance. The stability analysis for these non-unique solutions was consequently omitted from this section.

Table 1: Thermophysical properties of water-based and ferroparticles (Ramli *et al.*, 2018; Ramli & Ahmad, 2021)

Thermophysical Properties	Water-based	Ferroparticles		
		Fe_3O_4	$CoFe_2O_4$	$Mn-ZnFe_2O_4$
C_p (J/kg·K)	4,179	670	700	800
ρ (kg/m^3)	997	5,180	4,907	4,900
k (W/m·K)	0.613	9.7	3.7	5
σ (m^2/s)	5.5×10^{-6}	0.74×10^{6}	3.9×10^{6}	8×10^{6}

Table 2: Comparison of $f''(0)$ for $S = 3$ when Pr = 0.7, $\lambda = -1$, and M = Ec = R = 0

	Waini *et al.* (2019)		Yashkun *et al.* (2020)		Present Result	
	First Solution	Second Solution	First Solution	Second Solution	First Solution	Second Solution
$f''(0)$	2.390814	-0.972247	2.390813	-0.972247	2.390814	-0.972248

Figures 2 and 3 depict the impact of M on $f''(0)$ and $-\theta'(0)$ with λ when $\varphi = 0.1$, Pr = 6.2, $R = 1$, Ec = 1, $S = 3$, and $\gamma = 1$. It shows an increment in $f''(0)$ and $-\theta'(0)$ when M rises from 0 to 1 for the first solution and a reduction for the second solution. The Lorentz force provides the flow resistance, which is directly proportional to M. M describes the magnetic force applied to the medium. This magnetic force, on the other hand, reciprocates the electromagnetic force to viscous force ratio. An increase in M causes the magnetic field to gain power more quickly (Mishra & Kumar, 2020).

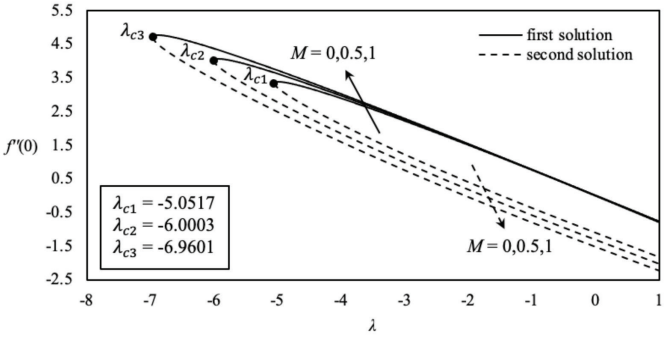

Figure 2: Diversity of $f''(0)$ with respect to λ for different values of M

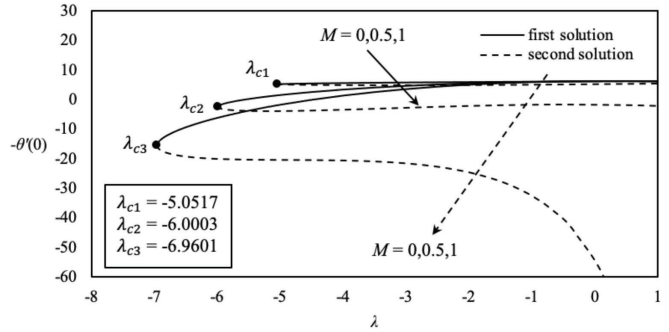

Figure 3: Diversity of $-\theta'(0)$ with respect to λ for different values of M

Meanwhile, Figures 4 and 5 present the effects of S, which are focusing only on suction on $f''(0)$ and $-\theta'(0)$ with λ when $M = 1$, $\varphi = 0.1$, Pr = 6.2, $R = 1$, Ec = 1, and $\gamma = 1$. For the first solution, $f''(0)$ and $-\theta'(0)$ increase with an increase in S. The tendency, however, is exactly the opposite for the second option. The rate of heat transfer accelerates in the presence of suction. Rather, suction contributes significantly to the system's improved cooling and may assist in postponing the shift from laminar flow. Delaying boundary layer separation is frequently required to minimise drag and achieve high lift values.

The consequence of M on the velocity $f'(\eta)$ and temperature $\theta(\eta)$ profiles is illustrated in Figures 6 and 7 when $\varphi = 0.1$, Pr = 6.2, $R = 1$, Ec = 1, $S = 3$, $\lambda = -5$, and $\gamma = 1$. The velocity profile and the thickness of the boundary layer are shown to be accelerating functions of M for the first solution. Considering that M's Lorentz force grows as it ascends, adding to the flow's resistance. On the other hand, an increase in M results in a rise in the temperature profile and thermal boundary thickness. The boundary layer thicknesses of the first and second solutions are different. It is clear that M affects the temperature and velocity profiles oppositely.

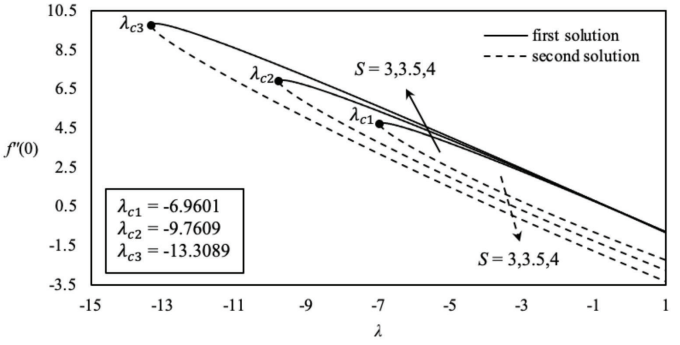

Figure 4: Diversity of $f''(0)$ with respect to λ for different values of S

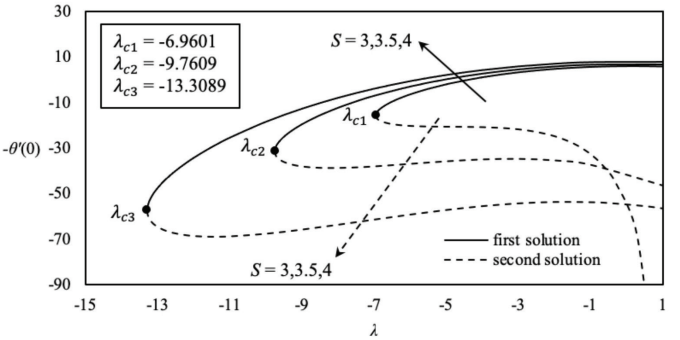

Figure 5: Diversity of $-\theta'(0)$ with respect to λ for different values of S

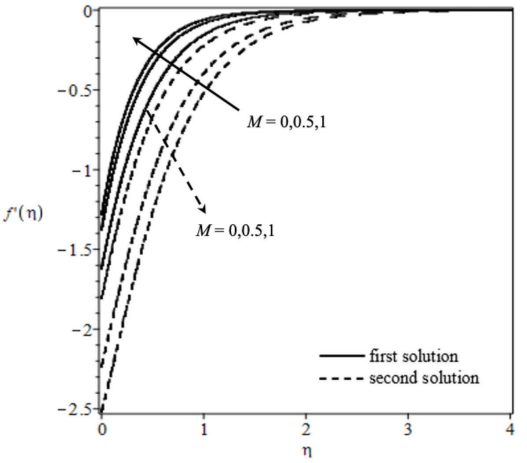

Figure 6: M's on the velocity profile

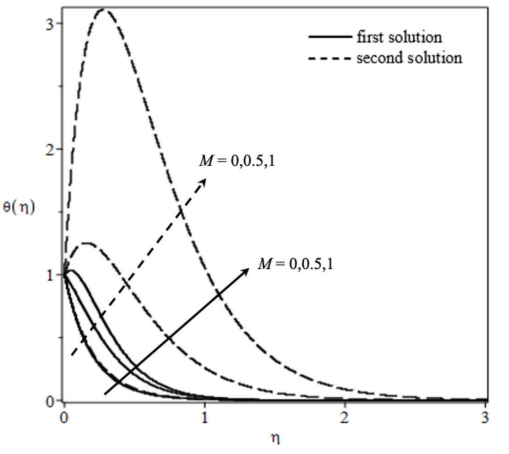

Figure 7: M's effect on the temperature profile

Figures 8 and 9 are plotted for the effects of S on the $f'(\eta)$ and $\theta(\eta)$ when $M = 1$, $\varphi = 0.1$, Pr = 6.2, $R = 1$, Ec = 1, $\lambda = -5$, and $\gamma = 1$. It is obvious that an increasing S causes the temperature profile to drop and the fluid velocity to rise. A suction technique is recommended if cooling is necessitated because it potentially makes the system cool down by the decrement of thermal layer.

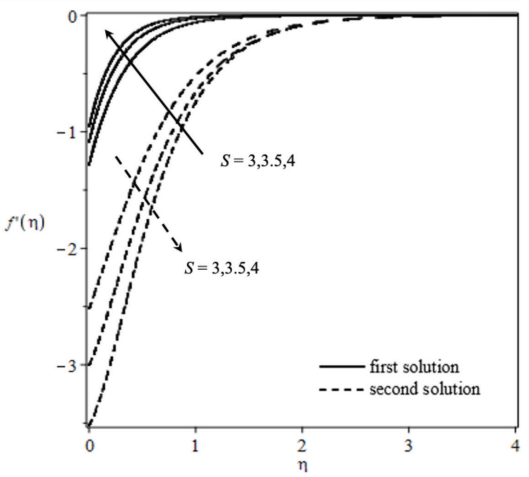

Figure 8: *S*'s effect on the velocity profile

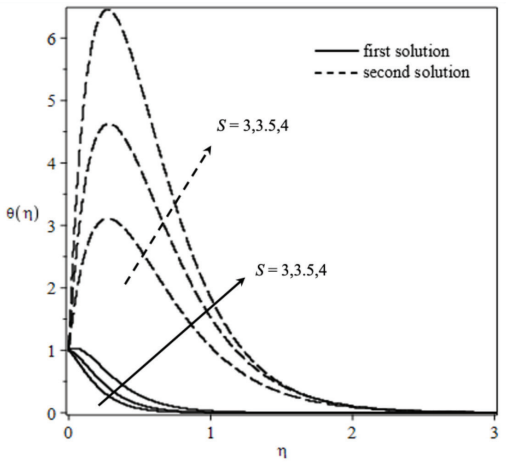

Figure 9: *S*'s effect on the temperature profile

The behaviour of Eckert number $\theta(\eta)$ against is depicted in Figure 10 when M = 1, φ = 0.1, Pr = 6.2, R = 1, S = 3, λ = -5, and γ = 1. Enthalpy and kinetic energy are correlated, so an increase in causes a corresponding rise in kinetic energy, further accelerating molecular motion and boosting temperature. The fluid flow will typically receive additional heat when Ec is improved, aiding in raising temperature.

Additionally, the impacts of thermal radiation parameter R on temperature are shown in Figure 11 for M = 1, φ = 0.1, Pr = 6.2, R = 1, S = 3, Ec = 1, λ = -5, and γ = 1. The fluid temperature was shown to rise due to R and as a result, the thermal boundary layer thickness tends to rise. The association between thermal boundary layer and temperature is elucidated physically by their relationship, which is directly proportional. This agrees with the empirical observation that the thermal boundary width expands as R grows (Goud *et al.*, 2020).

Figures 12 and 13 elucidate the influence of the γ on the velocity and temperature profiles when M = 1, φ = 0.1, Pr = 6.2, R = 1, Ec = 1, S = 3, and λ = 1. These graphs demonstrate that as γ is increased, $f'(\eta)$ decreases, and $\theta(\eta)$ rises. This is because velocity slip slows fluid motion in a manner that essentially confirms a reduction in

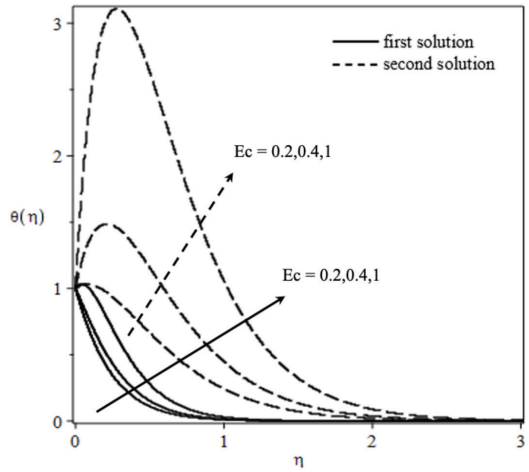

Figure 10: Ec's effect on the temperature profile

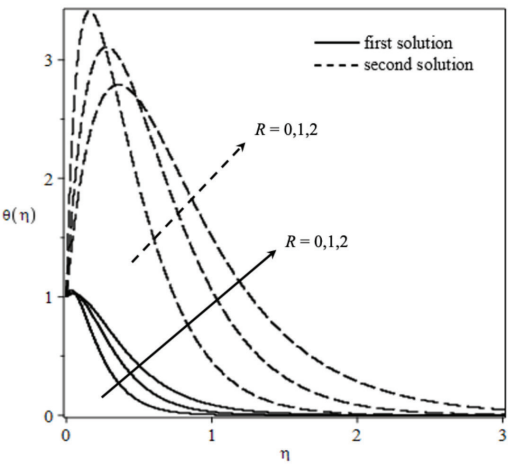

Figure 11: *R*'s effect on the temperature profile

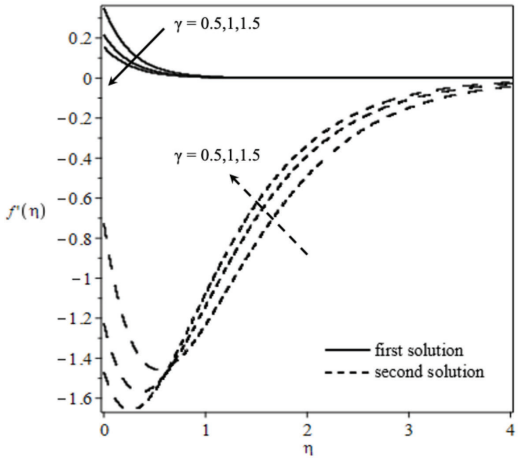

Figure 12: γ's effect on the velocity profile

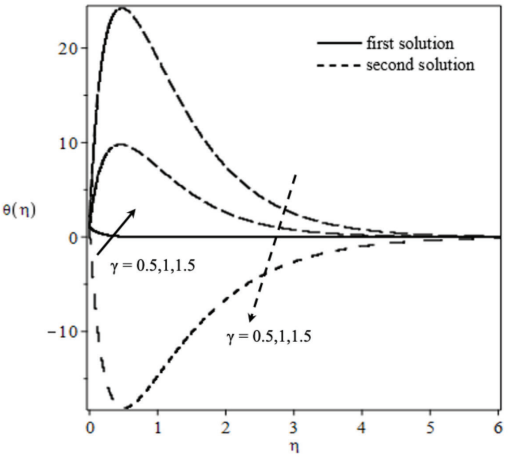

Figure 13: γ's effect on the temperature profile

the net movement of fluid molecules. Decreased molecular mobility thus leads to reduced velocity fields (Hayat *et al.*, 2014).

When trying to speed up heat transmission, the type of ferrofluid is perhaps one of the most crucial considerations. In order to determine which ferroparticle has the highest cooling capability, several of them are compared. Table 3 displays the impact of various kinds of ferrofluids on $f''(0)$ and $-\theta'(0)$ with $M = 0.5$, $\varphi = 0.1$, $S = 3$, $R = 1$, Ec = 1, and $\gamma = 1$ with the values of stretching ($\lambda = 1$) and shrinking ($\lambda = -1$) cases. The outcome reveals that extending a case transmits heat faster than shrinking a case. Additionally, we can observe from this table that the cobalt ferrite ferroparticle, $CoFe_2O_4$ has the largest local Nusselt number compared to other ferroparticles, leading to the highest heat transmission rate. According to Table 3, $CoFe_2O_4$ has the smallest thermal conductivity value compared to other ferroparticles. As a result, a reduction in $CoFe_2O_4$'s thermal conductivity could result in higher temperature gradients and better heat transfer outcomes.

Conclusions

The issue of ferrofluid MHD flow and heat transmission over an exponential stretching or shrinking in the presence of Joule heating and thermal radiation on slip was addressed in the current study. Before numerical analysis by shooting technique, the governing equations of non-linear PDEs were translated into ODEs. The results were compared to the literature

Table 3: Variation of $f''(0)$ and $-\theta'(0)$ with λ for different ferroparticles with water-based when $M = 0.5$, $\varphi = 0.1$, $R = 1$, Ec = 1, $S = 3$, and $\gamma = 1$

λ	Ferroparticle	$f''(0)$		$-\theta'(0)$	
		First Solution	Second Solution	First Solution	Second Solution
-1	Fe_3O_4	0.7681	-0.5869	5.9341	-1.8325
	$CoFe_2O_4$	0.7647	-0.5666	6.2825	-1.5258
	$Mn-ZnFe_2O_4$	0.7646	-0.5661	6.2187	-1.4637
1	Fe_3O_4	-0.7788	-2.0310	6.1359	-2.2106
	$CoFe_2O_4$	-0.7759	-2.0019	6.4931	-1.8737
	$Mn-ZnFe_2O_4$	-0.7758	-2.0012	6.4285	-1.8198

and the numerical results closely resemble the previously published results. Following is a summary of the main ideas:

- It has been noticed that dual solutions to the stretching or shrinking issue exist for a particular range.
- As the magnetic parameter *M* increases, the skin friction coefficient and heat transfer rate also rise. A stronger *M* causes an increase in temperature and velocity.
- In the presence of suction, the rate of heat transfer increases.
- The impacts of the radiation parameter *R* and the Eckert number Ec, respectively, led to a rise and improvement in the temperature distributions.
- The slip parameter was investigated to reduce skin friction and accelerate heat transfer.
- Heat transmission occurs more quickly in stretching circumstances than in shrinking cases.
- The cobalt ferrite ferroparticle in the water-based ferrofluid has the maximum heat transfer rate compared to magnetite and manganese-zinc ferrite.
- The heat transfer rate can be sped up by maximising the Eckert number's values and those of the radiation, magnetic, and slip parameters.

Acknowledgements

The authors would like to express their sincere gratitude to Universiti Sains Malaysia for their financial assistance (grant number: 304/PMATHS/6315383).

Conflict of Interest Statement

The authors declare that they have no conflict of interest.

References

Abbas, Z., Perveen, R., Sheikh, M., & Pop, I. (2016). Thermophoretic diffusion and nonlinear radiative heat transfer due to a contracting cylinder in a nanofluid with generalised slip condition. *Results in Physics*, *6*, 1080-1087. https://doi.org/10.1016/j.rinp.2016.11.049

Abdel-Wahed, M. (2017). Rotating ferro-nanofluid over stretching plate under the effect of Hall current and Joule heating. *Journal of Magnetism and Magnetic Materials*, *429*, 287-293. https://doi.org/10.1016/j.jmmm.2017.01.032

Abrar, M. N., Sagheer, M., & Hussain, S. (2019). Entropy formation analysis for the peristaltic motion of ferrofluids in the presence of Joule heating and fluid friction phenomena in a plumb duct. *Journal of Nanofluids*, *8*, 1305-1313. https://doi.org/10.1166/jon.2019.1672

Alsaady, M., Fu, R., Li, B., Boukhanouf, R., & Yan, Y. (2015). Thermo-physical properties and thermo-magnetic convection of ferrofluid. *Applied Thermal Engineering*, *88*, 14-21. https://doi.org/10.1016/j.applthermaleng.2014.09.087

Aly, E. H., & Ebaid, A. (2013). Exact analytical solution for suction and injection flow with thermal enhancement of five nanofluids over an isothermal stretching sheet with effect of the slip model. *Abstract and Applied Analysis*, *2013*(3), 1-14. http://dx.doi.org/10.1155/2013/721578

Anuar, N. S., Bachok, N., & Pop, I. (2021). Influence of MHD hybrid ferrofluid flow on exponentially stretching/shrinking surface with heat source/sink under stagnation point region. *Mathematics*, *9*, Article 2932. https://doi.org/10.3390/math9222932

Asadi, A., Nezhad, A. H., Sarhaddi, F., & Keykha, R. (2019). Laminar ferrofluid heat transfer in presence of non-uniform magnetic field in a channel with sinusoidal wall: A numerical study. *Journal of Magnetism and*

Magnetic Materials, *471*, 56-63. https://doi.org/10.1016/j.jmmm.2018.09.045

Babu, M. J., Sandeep, N., Raju, C. S. K., Reddy, J. V. R., & Sugunamma, V. (2016). Nonlinear thermal radiation and induced magnetic field effects on stagnation-point flow of ferrofluids. *Journal of Advanced Physics*, *5*, 302-308. http://dx.doi.org/10.1166/jap.2016.1271

Blaney, L. (2007). Magnetite (Fe_3O_4): Properties, synthesis, and applications. *Lehigh Review*, *15*, 33-68. https://ferrocell.us/references/Magnetite%20(Fe_3O_4)_%20Properties%20Synthesis%20and%20Applications.pdf

Cao, Y., Mansir, I. B., Singh, P. K., Ali, H. E., Abed, A. M., El-Refaey, A. M., Aly, A. A., Nguyen, D. T., Wae-hayee, M., & Tran, D. C. (2023). Heat transfer analysis on ferrofluid natural convection system with magnetic field. *Ain Shams Engineering Journal*, *14*, 102122. https://doi.org/10.1016/j.asej.2023.102122

Chamkha, A. J., Mujtaba, M., Quadri, A., & Issa, C. (2003). Thermal radiation effects on MHD forced convection flow adjacent to a non-isothermal wedge in the presence of a heat source or sink. *Heat and Mass Transfer*, *39*, 305-312. https://doi.org/10.1007/s00231-002-0353-4

Fadaei, F., Shahrokhi, M., Dehkordi, A. M., & Abbasi, Z. (2017). Heat transfer enhancement of Fe_3O_4 ferrofluids in the presence of magnetic field. *Journal of Magnetism and Magnetic Materials*, *429*, 314-323.

Farooq, U., Hassan, A., Fatima, N., Imran, M., Alqurashi, M.S., Noreen, S., Akgl, A., & Bariq, A. (2023). A computational fluid dynamics analysis on Fe_3O_4 - H_2O based nanofluid axisymmetric flow over a rotating disk with heat transfer enhancement. *Scientific Reports*, *13*, Article 4679. https://doi.org/ 10.1038/s41598-023-31734-1

Gerdroodbary, M. B., Jafaryar, M., Sheikholeslami, M., & Amini, Y. (2023). The efficacy of magnetic force on thermal performance of ferrofluid in a screw tube. *Case Studies in Thermal Engineering*, *49*, Article 103187. https://doi.org/10.1016/j.csite.2023.103187

Goud, B. S., Reddy, Y. D., Rao, V. S. & Khan, Z. H. (2020). Thermal radiation and joule heating effects on a magnetohydrodynamic Casson nanofluid flow in the presence of chemical reaction through a non-linear inclined porous stretching sheet. *Journal of Naval Architecture and Marine Engineering*, *17*, 143-64. http://dx.doi.org/10.3329/jname.v17i2.49978

Gui, N. G. J., Stanley, C., Nguyen, N. T., & Rosengarten, G. (2018). Ferrofluids for heat transfer enhancement under an external magnetic field. *International Journal of Heat and Mass Transfer*, *123*, 110-121.

Hayat, T., Qayyum, A., & Alsaedi, A. (2014). Effect of heat and mass transfer in flow along a vertical stretching cylinder with slip conditions. *The European Physical Journal Plus*, *129*(4), Article 63. https://doi.org/10.1140/epjp/i2014-14063-9

Jamaludin, A., Naganthran, K., Nazar, R., & Pop, Ioan. (2020). Thermal radiation and MHD effects in the mixed convection flow Fe_3O_4 -water ferrofluid towards a nonlinearly moving surface. *Processes*, *8*, Article 95. https://doi.org/10.3390/pr8010095

Jue, T. C. (2006). Analysis of combined thermal and magnetic convection ferrofluid flow in a cavity. *International Communications in Heat and Mass Transfer*, *33*, 846-852. https://doi.org/10.1016/j.icheatmasstransfer.2006.02.001

Jusoh, R., Nazar, R., & Pop, I. (2018). Magnetohydrodynamic rotating flow and heat transfer of ferrofluid due to an exponentially permeable stretching/shrinking sheet. *Journal of Magnetism and Magnetic Materials*, *465*, 365-374. https://doi.org/10.1016/j.jmmm.2018.06.020

Khashi'ie, N. S., Wahid, N. S, Md Arifin, N., & Pop, I. (2022). Insight into three-

dimensional flow of three different dynamics of nanofluids subject to thermal radiation: The case of water-cobalt ferrite, water-manganese-zinc ferrite, and water-magnetite. *Heat Transfer*, *51*(5), 4434-4450. https://doi.org/10.1002/htj.22506

Khosravi, A., Malekan, M., & Assad, M. E. H. (2019). Numerical analysis of magnetic field effects on the heat transfer enhancement in ferrofluids for a parabolic trough solar collector. *Renewable Energy*, *134*, 54-63. https://doi.org/10.1016/j.renene.2018.11.015

Kumar, P. B. S., Gireesha, B. J., Mahanthesh, B., & Gorla, R. S. R. (2017). Radiative nonlinear 3D flow of ferrofluid with joule heating, convective condition, and Coriolis Force. *Thermal Science and Engineering Progress*, *3*, 88-94. https://doi.org/10.1016/j.tsep.2017.06.006

Kumar, V., Casel, M., Dau, V., & Woodfield, P. (2021). Effect of axisymmetric magnetic field strength on heat transfer from a current-carrying micro-wire in ferrofluid. *International Journal of Thermal Sciences*, *167*, 106976. https://doi.org/10.1016/j.ijthermalsci.2021.106976

Lajvardi, M., Moghimi-Ras. J., Hadi, I., Gavili, A., Isfahani T. D., Zabihi, F., & Sabbaghzadeh, J. (2010). Experimental investigation for enhanced ferrofluid heat transfer under magnetic field effect. *Journal of Magnetism and Magnetic Materials*, *322*(21), 3508-3513. https://doi.org/10.1016/j.jmmm.2010.06.054

Mat Yasin, M. H., Ishak, A., & Pop, I. (2015). MHD stagnation-point flow and heat transfer with effects of viscous dissipation, Joule heating and partial velocity slip. *Scientific Reports*, *5*, Article 17848. https://doi.org/10.1038/srep17848

Mishra, A., & Kumar, M. (2020). Velocity and thermal slip effects on MHD nanofluid flow past a stretching cylinder with viscous dissipation and Joule heating. *Springer Nature Applied Sciences*, *2*, Article 1350. https://doi.org/10.1007/s42452-020-3156-7

Mittal, A. S., Patel, H. R., & Darji, R. R. (2019). Mixed convection micropolar ferrofluid flow with viscous dissipation, Joule heating and convective boundary conditions. *International Communications in Heat and Mass Transfer*, *108*, 104320. https://doi.org/10.1016/j.icheatmasstransfer.2019.104320

Mustafa, M., Mushtaq, A., Hayat, T. & Alsaedi, A. (2016). Rotating flow of magnetite-water nanofluid over a stretching surface inspired by non-linear thermal radiation. *PLOS ONE*, *11*(2), e0149304.

Olayemi, O. A., Obalalu, A. M., Odetunde, C. B., & Ajala, O. A. (2022). Heat transfer enhancement of magnetised nanofluid flow due to a stretchable rotating disk with variable thermophysical properties effects. *The European Physical Journal Plus*, *137*, Article 393.

Raj, K., & Moskowitz, R. (1990). Commercial applications of ferrofluids. *Journal of Magnetism and Magnetic Materials*, *85*, 233-245.

Raju, C. S. K., Sandeep, N., Sulochana, C., & Sugunamma, V. (2015). Effects of aligned magnetic field and radiation on the flow of ferrofluids over a flat plate with non-uniform heat source/sink. *International Journal of Science and Engineering*, *8*(2), 151-158.

Raju, C. S. K., & Sandeep, N. (2016). The effect of thermal radiation on MHD ferrofluid flow over a truncated cone in the presence of non-uniform heat source/sink. *Global Journal of Pure and Applied Mathematics*, *12*(1), 8-15.

Rashad, A. M. (2017). Impact of thermal radiation on MHD slip flow of a ferrofluid over a non-isothermal wedge. *Journal of Magnetism and Magnetic Materials*, *422*, 25-31.

Ramli, N., Ahmad, S., & Pop, I. (2017). Slip effects on MHD flow and heat transfer of ferrofluids over a moving flat plate. *AIP Conference Proceedings*, *1870*, 040015.

Ramli, N., Ahmad, S., & Pop, I. (2018). MHD forced convection flow and heat transfer of ferrofluids over a moving flat plate with uniform heat flux and second-order slip effects. *Scientia Iranica B*, *25*(4), 2186-2197.

Ramli, N., & Ahmad, S. (2019). Stability analysis of MHD mixed convection flow over a moving flat plate in ferrofluids with thermal radiation, suction and second-order slip effects: Heat flux case. *AIP Conference Proceedings*, *2184*, 060036.

Ramli, N., & Ahmad, S. (2021). Stability analysis of magnetohydrodynamic mixed convection flow and heat transfer over a moving flat plate in ferrofluids with suction and slip effects. *Modelling*, *Simulation and Applications of Complex Systems*, *Springer Proceedings in Mathematics and Statistics*, *359*, 233-250.

Rasli, N., & Ramli, N. (2021). Magnetohydrodynamic flow and heat transfer over an exponentially stretching/shrinking sheet in ferrofluids. *Pertanika Journal of Science and Technology*, *29*(3), 1811-1829.

Reddy, M. G. (2014). Influence of magnetohydrodynamic and thermal radiation boundary layer flow of a nanofluid past a stretching sheet. *Journal of Scientific Research*, *6*, 257-272.

Reddy, J. V. R., Sugunamma, V., & Sandeep, N. (2018). Combined effects of frictional and Joule heating on MHD nonlinear radiative Casson and Williamson ferrofluid flows with temperature dependent viscosity. *International Journal of Applied and Computational Mathematics*, *4*, Article 140.

Rosensweig, R. E. (1985). *Ferrohydrodynamics* (pp. 368). Cambridge University Press. https://doi.org/10.1063/1.1711103

Sajid, M., Iqbal, S. A., Naveed, M., & Abbas, Z. (2016). Joule heating and magnetohydrodynamic effects on ferrofluid (Fe_3O_4) flow in a semi-porous curved channel. *Journal of Molecular Liquids*, *222*, 1115-1120.

Shah, S., Hussain, S., & Sagheer, M. (2016). MHD effects and heat transfer for the UCM fluid along with Joule Heating and thermal radiation using Cattaeo-Chrisov heat flux model. *American Institute of Physics Advances*, *6*, 085103.

Sharifi, I., Shokrollahi, H., & Amiri, S. (2012). Ferrite-based magnetic nanofluids used in hyperthermia applications. *Journal of Magnetism and Magnetic Materials*, *324*(6), 903-915.

Sheikholeslami, M., & Shehzad, S.A. (2017). Thermal radiation of ferrofluid in existence of Lorentz forces considering variable viscosity. *International Journal of Heat and Mass Transfer*, *109*, 82-92.

Siddiqui, M. A., Javed, T., & Iftikhar, B. (2023). Augmenting the energy transport through magnetic ferrofluid filled inside the I-Shaped cavity under the influence of thermal radiation. *Journal of Nanofluids*, *12*, 745-758.

Stephen, P. S. (1965). *Low viscosity magnetic fluid obtained by the colloidal suspension of magnetic particles* (Patent No. 3,215,572). Google Patents. https://patents.google.com/patent/US3215572A/en

Wan Rosli, W. M. H., Mohamed, M. K. A., Md Sarif, N., Mohammad, N. F., & Soid, S. K. (2023). Boundary layer flow of Williamson hybrid ferrofluid over a permeable stretching sheet with thermal radiation effects. *CFD Letters*, *15*, Article 3.

Waini, I., Ishak, A., & Pop, I. (2020). Hybrid nanofluid flow induced by an exponentially shrinking sheet. *Chinese Journal of Physics*, *68*, 468-482.

Yashkun, U., Zaimi, K., Ishak, A., Pop, I., & Sidaoui, R. (2020). Hybrid nanofluid

flow through an exponentially stretching/shrinking sheet with mixed convection and joule heating. *International Journal of Numerical Methods for Heat and Fluid Flow*, *31*(6), 1930-1950. https://doi.org/10.1108/HFF-07-2020-0423

Zainodin, S., Jamaludin, A., Nazar, R., & Pop, I. (2022). MHD mixed convection of hybrid ferrofluid flow over an exponentially stretching/shrinking surface with heat source/sink and velocity slip. *Mathematics*, *10*, Article 4400. https://doi.org/10.3390/math10234400